13

Multilayer mirrors based on Cr/Ti for X-Ray microscopy in the „water window“

© S.A. Garakhin,[1] E.S. Antyushin,[1] M.M. Barysheva,[1,2] A.E. Pestov,[1] V.N. Polkovnikov,[1] R.S. Pleshkov,[1] R.M. Smertin,[1] N.I. Chkhalo[1]

[1] Institute of Physics of Microstructures, Russian Academy of Sciences,
607680 Afonino, Nizhny Novgorod, Russia
[2] Lobachevsky State University,
603022 Nizhny Novgorod, Russia
e-mail: garahins@ipmras.ru

Received May 13, 2024
Revised May 13, 2024
Accepted May 13, 2024

The impact of thin boron carbide (B_4C) layers on the internal structure and reflection coefficients of Cr/Ti multilayer mirrors at a wavelength of 2.74 nm Cr/Ti at normal incidence angles was studied. The mirrors had 400 periods of about 1.4 nm. The usage of interlayers made it possible to increase the reflection coefficients from 5% to 11% as a result of reduction the materials mixing at the interfaces. A significant part of the article is devoted to the issue of precision reflectometry using the laboratory reflectometer in the „water window“ spectral range.

Keywords: X-ray, multilayer mirrors, reflectometry, soft X-ray range, „water window“, interlayers, X-ray tube, diffraction grating, ion source.

DOI: 10.61011/TP.2024.08.59002.162-24

Introduction

Thanks to the rapid development of thin film sputtering technology, multilayer X-ray structures (MLS) have found wide application in various fields of science, engineering and technology. They are used in mass-produced X-ray diffractometers and spectrometers for monochromatization, focusing, and collimation of X-rays [1]. The crossed MLS system in the Kirkpatrick-Baez geometry ensures nanofocusing of synchrotron radiation [2]. MLS on transparent substrates or even free-hanging structures are used as beam splitters, polarizers, soft X-ray phase shifters, and filters for suppressing long-wave radiation [3–5] Recently, MLS have been actively used for X-ray microscopy [6,7] in the spectral region of the „water transparency window“, wavelengths of 2.3–4.4 nm. The wavelength range of $\lambda = 2.3-3.1$ nm remains the most problematic from the point of view of manufacturing multilayer optics: in this range, traditional weakly absorbing materials such as boron, carbon, and silicon have a quite strong absorption, so multilayer structures based on them have low reflection coefficients — less than 10%. High reflection coefficients can theoretically be achieved only in the regions of anomalous dispersion of the optical constants Ti ($\lambda = 2.74$ nm) for Cr/Ti-based structures [8] or V ($\lambda = 2.4$ nm) for structures of the type Cr / V [9].

This paper covers the study of Cr/Ti multilayer structures, including those with B_4C interlayers, optimized for the wavelength of $\lambda = 2.74$ nm. Previously, the maximum reflection coefficient of soft X-ray radiation with a wavelength of 2.74 nm (452 eV) for Cr/Ti structures was $R = 2.1\%$ at a near-normal incidence ($\sim 78.8^\circ$) in [8] for a multilayer mirror containing 100 periods with a thickness of $d = 1.379$ nm (the ratio of layer thicknesses is 0.5). A reflection coefficient of $R = 4.3\%$ was achieved for a mirror containing 150 periods, designed for operation at Brewster's angle of 45°. A two-stage ion-beam assisted deposition was used to minimize the roughness and mixing of materials at the interface during magnetron sputtering. The best Cr/Ti reflection without specifying the wavelength and angle of incidence of radiation, at 17% is mentioned in Ref. [10]. However, the article does not provide enough information for other scientific groups to repeat the result, in particular, the angle of incidence is not specified, which is very important, since the reflection coefficients at grazing angles of incidence in this wavelength range are significantly, many times larger than at normal.

Interface engineering methods were used in this paper for increasing the reflection coefficients of Cr/Ti structures and improving the quality of interlayer boundaries, for which thin B_4C boron carbide interlayers were introduced into the structure, since it was previously noted that B_4C layers contribute to the formation of the structure ensuring a sharp interface. Thus, one can hope to select such thickness of B_4C buffer layer thickness so that the decrease of the reflection coefficient due to additional absorption is compensated by an increase of reflection due to reduction of mixing of materials. The interlayer was applied to the surface of both chromium and titanium films.

A significant part of this paper is devoted to the issue of precision reflectometry on a laboratory reflectometer due to

the extreme complexity of measuring reflection coefficients in this wavelength range.

1. Fabrication of multilayer X-ray mirrors

Multilayer Cr/Ti X-ray mirrors with B_4C buffer layers and without them are fabricated by magnetron sputtering in Ar medium at gas pressure of ~ 0.2 Pa. Mirrors are deposited on smooth silicon wafers for microelectronics with a root-mean-square roughness of ~ 0.2 nm.

Mirror deposition is performed using an unique magnetron sputtering unit developed and assembled at IPM RAS. The unit includes a pumping station, a vacuum chamber, an electronics unit, and a personal computer with an installed control program. Pumping is performed by a dry pre-vacuum pump and a turbomolecular pump with magnetic suspension and a capacity of 2000 L/s. The residual pressure of gases in the working chamber is at the level of $3 \cdot 10^{-5}$ Pa before sputtering. The pre-vacuum pump was removed from the laboratory to a separate technological room for isolation of noise and vibration.

The vacuum chamber is a cylindrical volume with a height of 0.5 m and a diameter of 1 m, inside which six circular planar magnetrons with a diameter of 150 mm are installed around the circumference, which makes it possible to produce multilayer structures containing up to 6 layers of different materials per period. Shaped precision diaphragms are provided above each magnetron that ensure uniform (or with a given distribution) deposition of sputtered materials on a solid substrate.

Each magnetron is a ring-discharge source. A sputtered material target with a diameter of 150 mm and a thickness of 2 to 8 mm is located on the surface, serving as a cathode. The magnetic system of the magnetron creates a constant magnetic field in the gap between the poles with the intensity $4-7 \cdot 10^{-2}$ T. Magnetron power sources are stabilized DC units developed by IPM RAS that allow varying the discharge current within 100–2000 mA at voltages from 100 to 500–600 V. „Balzers“ unit with a frequency of 13.56 MHz is used for high-frequency sputtering of targets. Magnetrons are cooled by water using a pump. Thermal contact of the target with the magnetron is provided by the „Viksint“ sealant with a copper filler. High-purity (99.998%) argon is used as the working medium. The working gas pressure in the process is $8-13 \cdot 10^{-2}$ Pa.

The sputtering rate can be controlled by changing the currents on the magnetrons, as well as the speed of the substrate passing over them. Typical values of the film growth rate are 0.1–1 nm/s.

In the case of fabrication of Cr/Ti MLS, including those with B_4C interlayers, sputtering was carried out with a direct current, the values of which for different targets are as follows: $I_{\mathrm{Cr}} = 0.3$ A, $I_{\mathrm{Ti}} = 0.3$ A, $I_{\mathrm{B_4C}} = 0.8$ A. The deposition rates were ~ 0.08 nm/s for Ti, ~ 0.1 nm/s for Cr and ~ 0.02 nm/s for B_4C. The thicknesses of the B_4C interlayer were 0.05, 0.1, and 0.15 nm. The thickness of B_4C layer means here the average increment of the structure period due to the addition of B_4C to Cr/Ti, the formation of a continuous B_4C layer is not assumed. Interlayers were deposited both on Cr–on–Ti boundary and on Ti–on–Cr boundary. The value of the MLS period was $d \sim 1.4$ nm, the number of periods was $N = 400$.

The joint fitting of reflection curves obtained at wavelengths of 0.154 and 2.74 nm using the Multifitting [11] software package is used for determining the structural parameters of multilayer structures — average film thicknesses and dispersion, interlayer roughness, and material densities. In addition to interface parameters, this program is used to restore electron density profiles based on the MLS depth.

2. Study of Cr/Ti multilayer mirrors at wavelength of 0.154 nm

Angular dependences of reflection coefficients at $\mathrm{Cu}K_{\alpha 1}$ 0.154 nm are measured using four-crystal high-resolution diffractometer PANalytical X'pert-PRO (the Netherlands). The diffractometer is provided with a goniometer with 6 degrees of freedom, which ensures angular scanning with an accuracy better than 0.001° at angles up to 100°, which is more than enough for MLS reflectometry when the operating angles are in the range of units of degrees. The main factors resulting in the broadening of the observed peaks are the finite spectral width and angular divergence of the probe beam. This broadening can be ignored since the measurements are performed on the $\mathrm{Cu}K_{\alpha 1}$ line, whose natural width is $4.4 \cdot 10^{-5}$ nm, at small grazing angles, $\theta \approx 1$. The angular divergence of the probe beam of the diffractometer is better than 0.0036° [12].

3. Study of Cr/Ti multilayer mirrors at operating wavelength of 2.74 nm

Measurements of the reflection coefficient on the line of Ti Lα $\lambda = 2.74$ nm (452.2 eV) [13] are performed using a laboratory reflectometer developed in IPM RAS [14]. The reflectometer consists of a radiation source module, a monochromator spectrometer RSM-500, and a goniometer camera. The device diagram is shown in Fig. 1.

The RSM-500 uses a spherical diffraction grating as its spectral element. Spherical gratings with radii of curvature 6 m (range 0.6–5 nm), 4 m (range 1.6–9 nm) and 2 m (range 4–50 nm) are depending on the radiation range of interest.

Thus, polychromatic radiation from the source (X-ray tube) through the entrance slit falls on the diffraction grating, after which, in accordance with the grating equation

$$\cos\alpha - \cos\beta = m\frac{\lambda}{D}, \quad (1)$$

where m — diffraction order, λ — wavelength and D — grating period, α and β — angles of incidence and

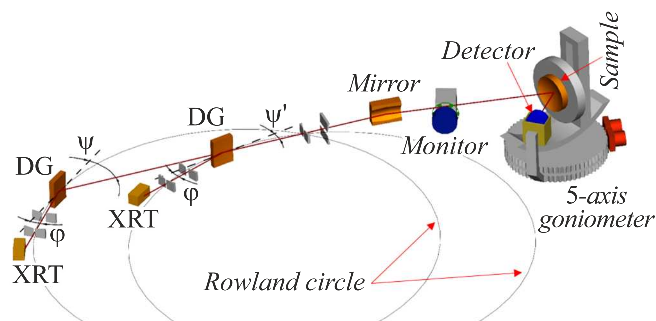

Figure 1. Diagram of a high-resolution laboratory reflectometer based on the RSM-500. XRT — X-ray tube, DG — spherical diffraction grating, Mirror — toroidal focusing mirror, Monitor, Detector — detectors SEM-6, Sample — example of a fixed sample.

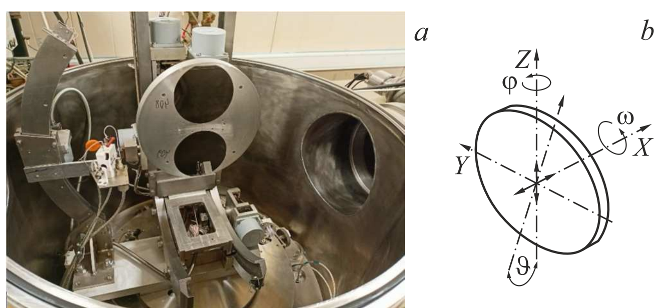

Figure 2. Image (*a*) of an open goniometer camera and a diagram of goniometer movements (*b*) of a high-resolution laboratory reflectometer based on RSM-500.

diffraction, respectively, monochromatic radiation is focused on the output slit of the spectrometer. Then the diffracted beam is directed through the output slit to a toroidal mirror that focuses radiation on the test sample mounted on the goniometer. The reflected radiation is detected by a detector based on a secondary electronic multiplier SEM-6. The anti-scattering horizontal and vertical diaphragms, which can be seen in Figure 1, serve to reduce the scattered radiation in the spectrometer, as well as to limit the vertical size of the probe beam.

Spectrum scanning is performed by shifting the diffraction grating blocks and the input slit (Fig. 1), while simultaneously rotating the diffraction grating. At the same time, the input and output slits and the diffraction grating move along a curved guide, strictly remaining on the Rowland circle, which simultaneously ensures high light intensity and spectral resolution of the device.

The diffraction grating and the source (input slit) are moving elements for spectrum scanning, the output slit is stationary. Thus, the goniometer camera is stationary, its size and weight are virtually unlimited. The test samples, the number of which is limited by the diameter of the sample holder disk 300 mm, are installed on the goniometer.

Image of the open goniometer camera and the goniometer itself, as well as a diagram of the goniometer movements, are shown in Figure 2. The goniometer used in the unit has 5 degrees of freedom: 1) rotation around the vertical axis; 2) rotation around the horizontal axis; 3) rotation around the axis perpendicular to the plane of the sample; 4) linear movement along the vertical axis; 5) linear movement along the axis perpendicular to the plane of the sample. All this makes it possible to study the optical properties at each point of a complex non-planar sample. The goniometer ensures an accuracy of linear displacements of 0.1 mm in the range of 150 mm along z and 50 mm along x axes; the accuracy of angular displacements of the sample and detector is not worse than 0.025°, deviation at the angles φ, 2φ can reach ±360°, at the angles ϑ, 2ϑ — ±30°. Also, the table can rotate around its axis by 360° with an accuracy of 0.1°, which increases the number of samples that can be examined without additional opening of the vacuum chamber.

The intensity of the probe beam can be monitored using a single-photon detector-monitor (Monitor), to which part of the X-ray beam is directed, or using the main detector, for which the sample is removed from the beam. A photocathode covered with a CsI layer sensitive to X-ray radiation is installed in front of the detector. The detector (secondary electron multiplier SEM-6) has two rotational degrees of freedom: rotation around the vertical and horizontal axes. The reference signal acts as a reference point for counting the angular position of the detector (the sample is taken out of the beam), then the angular position of the sample is corrected according to the maximum reflection in the 2φ-scanning diagram first in the region of the critical angle, then in the region of Bragg angle.

The goniometer chamber is stationary in the described reflectometer circuit, so the studied sample can be massive. However, the source that moved along the Rowland circle together with the diffraction grating should have small overall dimensions and weight. The laboratory reflectometer uses a demountable X-ray tube with a replaceable rotary anode as a radiation source [15]. The rotary 4-face anode assembly allows measurements on the characteristic lines of four different materials without exposing them to the atmosphere. The desired face is rotated in the direction of the cathode for selection of the anode material, which also increases the service life of the tungsten filament and ensures stability of the emission characteristics by reducing contamination of the target surface with products of thermal cathode evaporation and decomposition under the impact of an electron beam of bicarbones contained in the residual gas. 4 targets are soldered to a water-cooled copper holder in this experiment: magnesium (Mg), iron (Fe), titanium (Ti), and carbon (C). When these targets are used, the measurements are performed on the emission lines of materials whose intensity varies from 150–250 photons/s for titanium to 2500 photons/s for Mg. There are also replaceable 4-and 6-sided anode assemblies with various materials, for example, tungsten (W). In this case, work can

Structural parameters of Cr/Ti MLS with interlayers B_4C

Sample	Structure $N = 400$	d, nm	t, nm	Layer composition	ρ, g/cm^3	s, Å
192 (1)	Cr/Ti	1.41	Ti ~ 0.7 Cr ~ 0.7	$Ti_{1.0}Cr_{0.11}$ $Cr_{1.0}Ti_{0.26}$	4.9 6.8	3.6 3.4
203 (2)		1.38	B_4C ~ 0.01 Ti ~ 0.7 Cr ~ 0.7	$Ti_{1.0}Cr_{0.05}B_{0.04}C_{0.01}$ $Cr_{1.0}Ti_{0.06}B_{0.04}C_{0.01}$	4.5 6.9	3.6 3.4
206 (3)	Cr/Ti/B_4C	1.38	B_4C ~ 0.015 Ti ~ 0.7 Cr ~ 0.7	$Ti_{1.0}Cr_{0.02}B_{0.06}C_{0.015}$ $Cr_{1.0}Ti_{0.02}B_{0.06}C_{0.015}$	4.5 6.9	3.6 3.4
207 (4)		1.38	B_4C ~ 0.02 Ti ~ 0.7 Cr ~ 0.7	$Ti_{1.0}B_{0.08}C_{0.02}$ $Cr_{1.0}B_{0.08}C_{0.02}$	4.5 7.0	3.6 3.4
219 (5)		1.40	Ti ~ 0.7 B_4C ~ 0.01 Cr ~ 0.7	$Ti_{1.0}Cr_{0.04}B_{0.04}C_{0.01}$ $Cr_{1.0}Ti_{0.02}B_{0.04}C_{0.01}$	4.7 6.9	3.6 3.4
231 (6)	Cr/B_4C/Ti	1.39	Ti ~ 0.7 B_4C ~ 0.015 Cr ~ 0.7	$Ti_{1.0}Cr_{0.04}B_{0.06}C_{0.015}$ $Cr_{1.0}Ti_{0.02}B_{0.06}C_{0.015}$	4.5 6.9	3.6 3.4
220 (7)		1.39	Ti ~ 0.7 B_4C ~ 0.02 Cr ~ 0.7	$Ti_{1.0}B_{0.08}C_{0.02}$ $Cr_{1.0}B_{0.08}C_{0.02}$	4.4 6.9	3.6 3.4

Note. N — number of periods in MLS, d — MLS period, t — layer thickness, ρ — layer density, s — interface width.

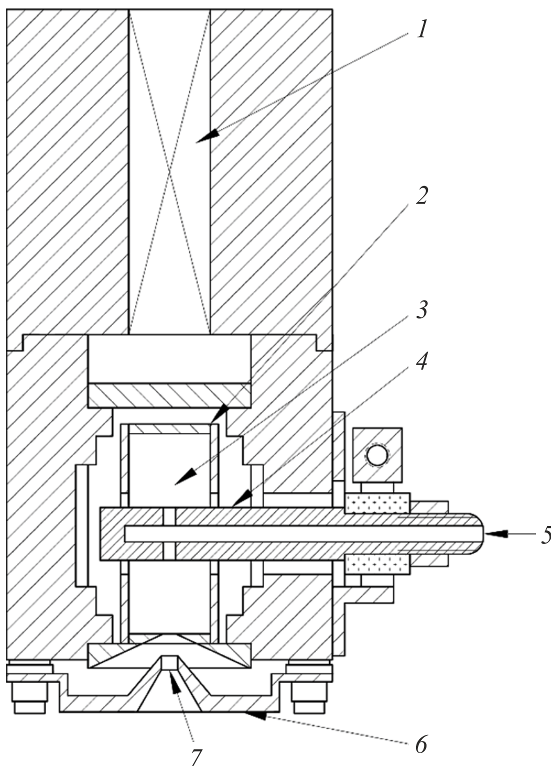

Figure 3. Ion source circuit: *1* — permanent magnet, *2* — cathode, *3* — discharge chamber, *4* — anode, *5* — gas inlet (Ar), *6* — accelerating electrode, *7* — output slit.

be performed on the bremsstrahlung spectrum, the photon power spectral density is 60–80 photons/(0.01 nm · s). Thus, with signal accumulation, it is not difficult to obtain a statistical measurement error of 1% over the entire wavelength range.

When X-ray tube anodes made of various materials are used, the operating wavelength range of a laboratory reflectometer from the short-wavelength part of the soft X-ray spectrum is limited only by the diffraction efficiency of the grating and is about 0.6 nm, with moderate energy consumption, at the level of tens-hundreds of W. In addition, there is no need for expensive, large-scale systems to protect the optical elements of the device from contamination caused by erosion flows from a laser-plasma or gas-discharge source [16].

One of the important advantages of the X-ray tube used in the reflectometer is the built-in ion source developed in IPM RAS and designed for cleaning the target (anticathode) from contamination by products of evaporation of the thermocathode material and decomposition of hydrocarbons and other residual gases.

The ion source diagram is shown in Figure 3. The operating principle of the source is as follows. The potential difference between the cathode *2* and the anode *4* is set to 1000 V, then the working gas Ar is supplied through the gas inlet channel *5* to the discharge chamber *3*. A gas breakdown occurs when the pressure in the chamber is $1 \cdot 10^{-3}$ Pa, an independent discharge lights up, and the discharge voltage (between the cathode and anode)

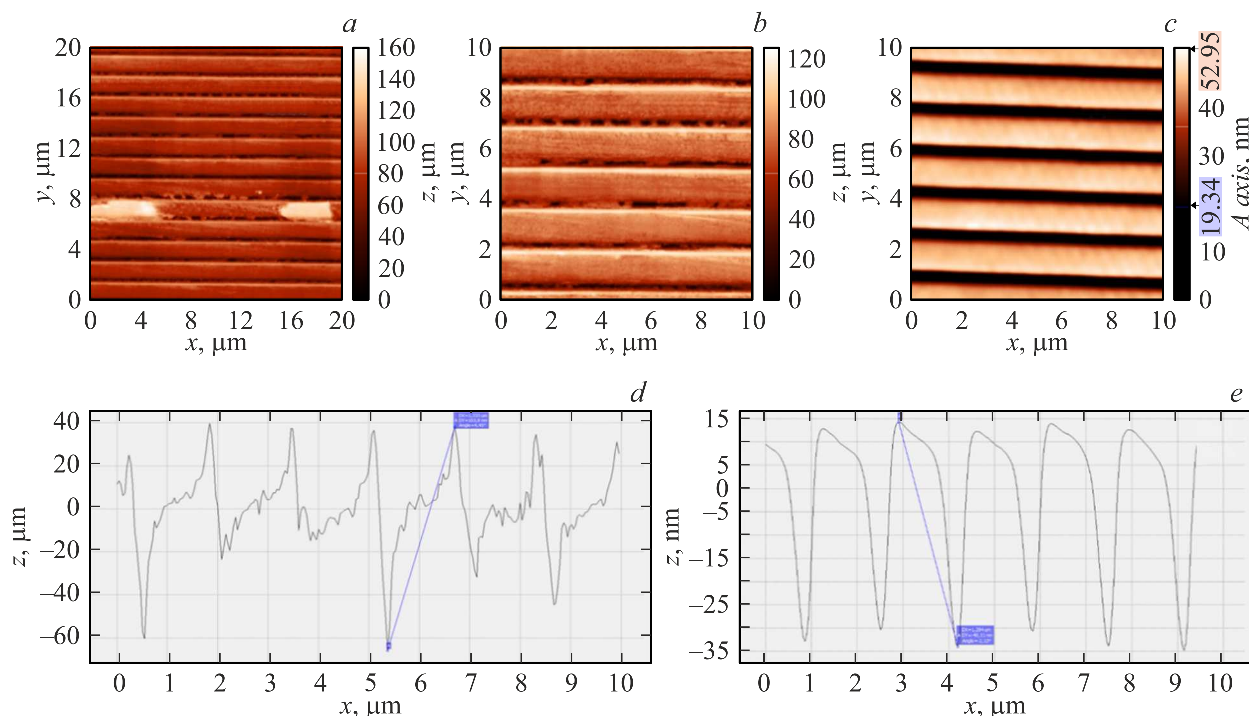

Figure 4. Results of AFM diffraction grating studies before (a, b, d) and after (c, e) ion polishing procedures. Blue lines in drawings (d, e) show the measured period 1.3 μm, with elevation differences of 103.8 and 48.11 nm, respectively.

decreases to 250 V. An accelerating voltage of 1250 V is applied to the accelerating electrode *6*, and an ion beam begins to exit from the output slit *7*. The profile of the accelerating electrode is calculated in such a way as to provide a quasi-uniform distribution of the ion current on the surface of the target of the X-ray tube. The surface contamination is etched within about 30 min.

The effect of ion etching is manifested not only in an increase in the lifetime of the X-ray tube and the productivity (there is no need to open the tube chamber to the atmosphere for mechanical cleaning or replacement of the target), but also in the stability of the emission characteristics of targets, which is most important for precision measurements.

A spherical diffraction grating with a radius of 6 m with a groove frequency of 600 lines/mm is used as a spectral device in this experiment. Initially, an echelle grating with a groove height of 15 nm had a large roughness of grooves, which reduced its efficiency at short wavelengths. Images of grating fragments obtained by atomic force microscopy (AFM) are shown in Fig. 4: frames 20 (*a*), 10 μm (*b*) and groove profile (*d*). The grating was subjected to ion etching with an ion beam for smoothing out the grating roughness. Etching was performed with argon (Ar) ions with an energy of 800 eV at the normal to the surface, and the current density was 0.4 mA/cm. The result of three polishing operations is shown in Fig. 4, *c, e*. When comparing AFM images (Fig. 4, *a*–*c*) and the grating profiles constructed from them (Fig. 4, *d, e*), it is clear that the quality of the reflecting surface has increased, and the groove has become closer to triangular.

After the ion etching procedure, the grating was coated with a platinum layer with a thickness of 30 nm. The study of the reflective characteristics of the grating fabricated using this procedure on the carbon CK_α 4.47 nm line at an angle of incidence of radiation on the grating of 2°, which corresponds to the grating installation scheme in RSM-500, showed mirror reflection at 30%, reflection in first-order diffraction of 10%.

Figure 5 shows the Ti target spectra recorded on a laboratory reflectometer in zero diffraction order and near the Ti L 2.74 and 3.14 nm spectral lines. It can be seen that the measured widths of these lines are 0.023 and 0.026 nm, respectively. The spectral width of the probe beam is one of the most important characteristics that affect the accuracy of measuring the absolute values of the peak reflection coefficients and the spectral resolution of the optics under study. In this case, the spectral resolution of the grating spectrometer is determined both by the individual properties of the diffraction grating and, to a large extent, by the alignment of the device. The inclination of the input and output slits relative to each other and relative to the reflecting plane of the diffraction grating, and the mismatch of the position of the slits and grating relative to the Rowland circle (violation of the focusing condition) are the main negative factors among the alignment errors. Since these factors are purely geometric in nature, appearing equally in the case of a diffraction image of a spectral

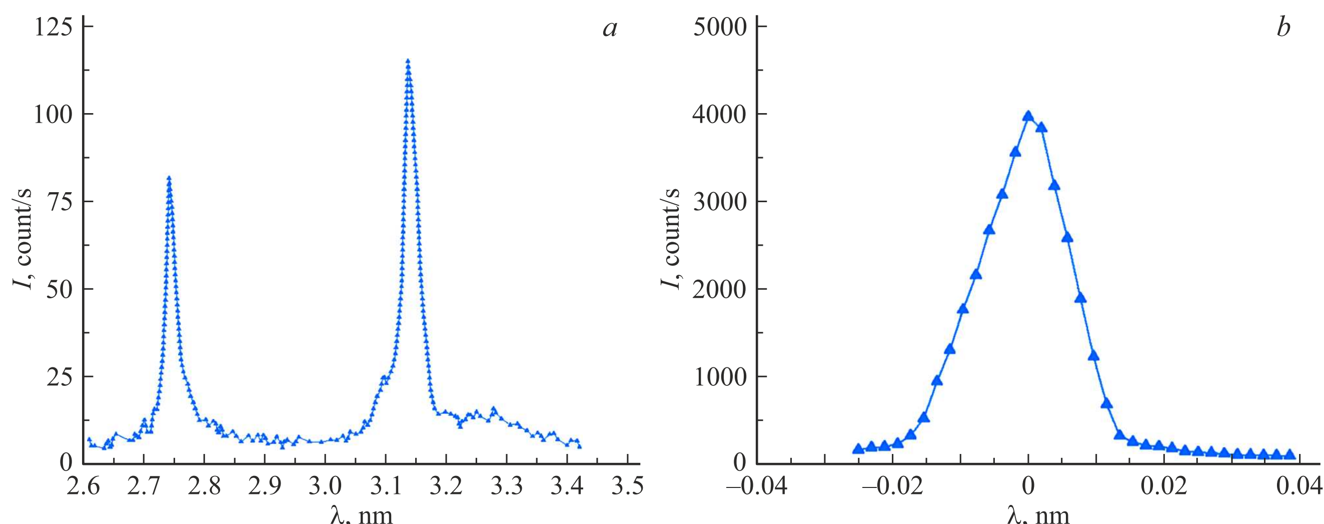

Figure 5. Spectral curves recorded using the laboratory reflectometer on a Ti target in zero diffraction order (*a*) and in the region of Ti 2.74 and 3.14 nm lines (*b*).

line and in the zero-order diffraction, as shown earlier in Ref. [12], the spectral resolution of the device can be reliably determined from the spectral width of the zero diffraction order and does not depend on the radiation wavelength.

Figure 5, *a* shows the spectral dependence of the X-ray beam intensity measured on the Ti target in zero diffraction order. Negative wavelengths imply a negative diffraction order according to the expression (1). The spectral line width measured with the spectral instrument, $\Delta\lambda^{\mathrm{Ti}}_{\mathrm{meas}}$, is related to the true line width, $\Delta\lambda^{\mathrm{Ti}}_{\mathrm{line}}$ and the width of the device instrument function $\Delta\lambda_{\mathrm{App}}$ by the relation

$$\Delta\lambda^{\mathrm{Ti}}_{\mathrm{meas}} = \Delta\lambda^{\mathrm{Ti}}_{\mathrm{line}} + \Delta\lambda_{\mathrm{App}}, \tag{2a}$$

if the spectral lines can be represented by Lorentz curves. This relationship is quadratic for Gaussian curves:

$$(\Delta\lambda^{\mathrm{Ti}}_{\mathrm{meas}})^2 = (\Delta\lambda^{\mathrm{Ti}}_{\mathrm{line}})^2 + (\Delta\lambda_{\mathrm{App}})^2. \tag{2b}$$

Having estimated the width of Ti lines according to these formulas from the measurement data (Fig. 5, *b*), we obtain, depending on the model used (Gaussian or Lorentz), the width of both lines at the level of $0.1-0.2$ nm.

Thus, in the case of measurements of the reflectometric characteristics of Cr/Ti X-ray mirrors on titanium lines, we have a situation where the apparatus function of the device is comparable in width to both the spectral line on which the measurements are made and, as will be shown below, to the spectral width of the reflection curves of Cr/Ti structures. Under such conditions, the reflection curves measured with a laboratory reflectometer will be noticeably distorted (broadened) in comparison, for example, with the results of synchrotron measurements, which are characterized by narrow spectral lines, and the peak reflection coefficient measured in laboratory conditions will be lower.

Therefore, for adequate measurements, it is necessary to establish the correct model for the apparatus function. We used two approaches. The first approach is based on comparing the results of zero-order measurements and narrow-line spectral measurements: AlK_α, 0.834 nm and FeL_α, 1.76 nm. The comparison results showed that the experimental data are better described using the Gaussian model.

The second approach was discussed earlier in Ref. [17] for Cr/Sc multilayer structures certified using a laboratory reflectometer and on BESSY-2 synchrotron facility at a wavelength of 3.14 nm. It was shown that the laboratory reflectance curve noticeably broadens, and the peak value of the reflectance coefficient measured on a laboratory reflectometer was $\cong 13\%$, the peak value of the reflectance coefficient measured using the synchrotron facility was $\cong 17\%$. It should be noted that the measurement of the reflection coefficients of multilayer X-ray mirrors on narrow spectral lines repeatedly showed that the results of preliminary laboratory measurements coincide well with the qualification data of the BESSY-II synchrotron facility [18–20].

It is possible to propose a method for estimating the real reflection coefficient of an X-ray mirror based on laboratory measurements taking the result of synchrotron measurements as a reference, comparing the reflection curves of X-ray radiation obtained on a laboratory reflectometer and in the synchrotron facility. In general, the relationship between the real reflection curve (the result of synchrotron measurements) of an X-ray mirror $R_{\mathrm{exp}}(\lambda)$ and the measured reflection curve $R_{\mathrm{meas}}(\theta)$ is given by the relation

$$R_{\mathrm{meas}}(\lambda) = \int\limits_{\lambda_{\min}}^{\lambda_{\max}} R_{\mathrm{exp}}(\lambda')A(\lambda-\lambda')d\lambda', \tag{3}$$

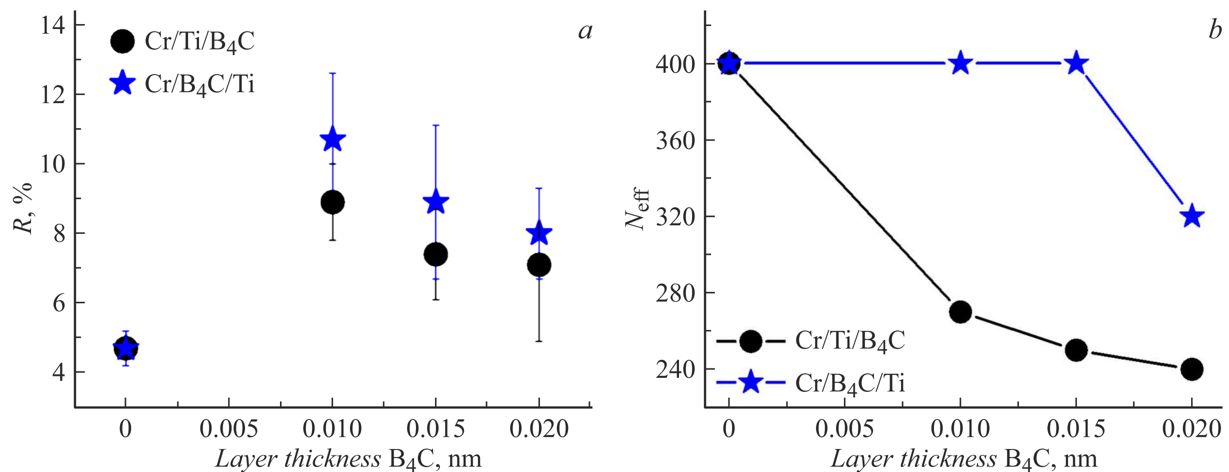

Figure 6. Dependence of the reflection coefficient (*a*) and the number N_{eff} on the thickness of B_4C buffer layers in MLS based on Cr/Ti (*b*).

where $A(\lambda-\lambda')$ is the instrument function of the reflectometer, normalized to one

$$\int_{\lambda_{\min}}^{\lambda_{\max}} A(\lambda)d\lambda = 1.$$

The measured reflection curve coincides with the real curve for a delta-like $A(\lambda-\lambda')$, which is true for synchrotron sources. Further, we will always assume that synchrotron measurements provide „true", the reference value of the reflection coefficient.

The study showed that the Gaussian model is the best model for accounting for the instrument function, therefore, a quadratic ratio is obtained between the measured $\Delta\lambda_{\text{meas}}$ and the real $\Delta\lambda_{\text{exp}}$ widths of reflection curves using the Gaussian approximation in (3), for the spectral widths of the reflection curves of X-ray mirrors, as in the case of (2b):

$$\Delta\lambda^2_{\text{meas}} = \Delta\lambda^2_{\text{exp}} + \Delta\lambda^2_{\text{App}}, \quad (4)$$

Thus, knowing the parameters of the instrument function, starting from the reflection curve obtained using a laboratory reflectometer, it is possible to obtain the value of the real peak reflection coefficient, which will correspond to the coefficient obtained by synchrotron measurements. The Bragg equation can be used to switch from spectral reflection coefficients to angular ones

$$2nd \sin\theta_{\max} = m\lambda \quad (m = 1), \quad (5)$$

where n is the average refractive index of the multilayer mirror and, thus,

$$\Delta\lambda/\lambda = \Delta\theta/\operatorname{tg}\theta_{\max}, \quad (6)$$

where $\theta_{\max}$ is the grazing angle corresponding to the reflection peak at a fixed wavelength, $\Delta\lambda$ and $\Delta\theta$ are the reflection peak widths for the spectral and angular curves, respectively. It is possible to estimate $R_{\text{exp}}\Delta\lambda_{\text{exp}} \cong R_{\text{meas}}\Delta\lambda_{\text{meas}}$ from the above ratios (an approximate representation of the integral), i.e. the reflection curve measured on a laboratory reflectometer shows a lower reflection coefficient and a larger width, which is observed in the experiment.

Thus, this ratio can be used to reconstruct the actual peak reflection coefficient based on the value obtained using a laboratory reflectometer: R_{meas} and $\Delta\theta_{\text{meas}}$ are taken from laboratory measurements, then (4) and (6) are used to calculate $\Delta\theta_{\text{exp}}$ and R_{exp}.

We obtained the width of the instrument function in the expressions (3), (4) at the level of $\Delta\lambda_{\text{App}} \cong 0.01$ nm by comparing the results of measurement of the reflection coefficient of Cr/Sc multilayer structures on a laboratory reflectometer and a BESSY-2 synchrotron facility at a Ti wavelength of 3.14 nm [17] and approximating the reflection curves and the instrument function of the reflectometer with Gaussian curves. Then, the real reflection characteristics of multilayer Cr/Ti structures in the soft X-ray range are estimated using formulas (4)–(6) and the MLS internal structure was restored using a joint fitting of the results of study of MLS in the soft and hard wavelength ranges, using Multifitting software package.

4. Results and discussion

This paper studies Cr/Ti MLS with B_4C interlayers with thicknesses of 0.01, 0.015 and 0.2 nm at different interface boundaries. The table shows the structural parameters of the best MLS studied based on the Cr/Ti pair, and the reflection coefficients at a wavelength of 2.74 nm are shown in Fig. 6, *a*. We obtained reflection coefficients at the level of $R = 4.7 \pm 0.5\%$ without using the B_4C layer for Cr/Ti MLS, with $N = 400$. Such a low reflectivity value is attributable to the strong mixing of the layers of the multilayer system with each other: Cr layers contain ~ 20 at.% Ti, and Ti layers contain ~ 10 at.%. This results

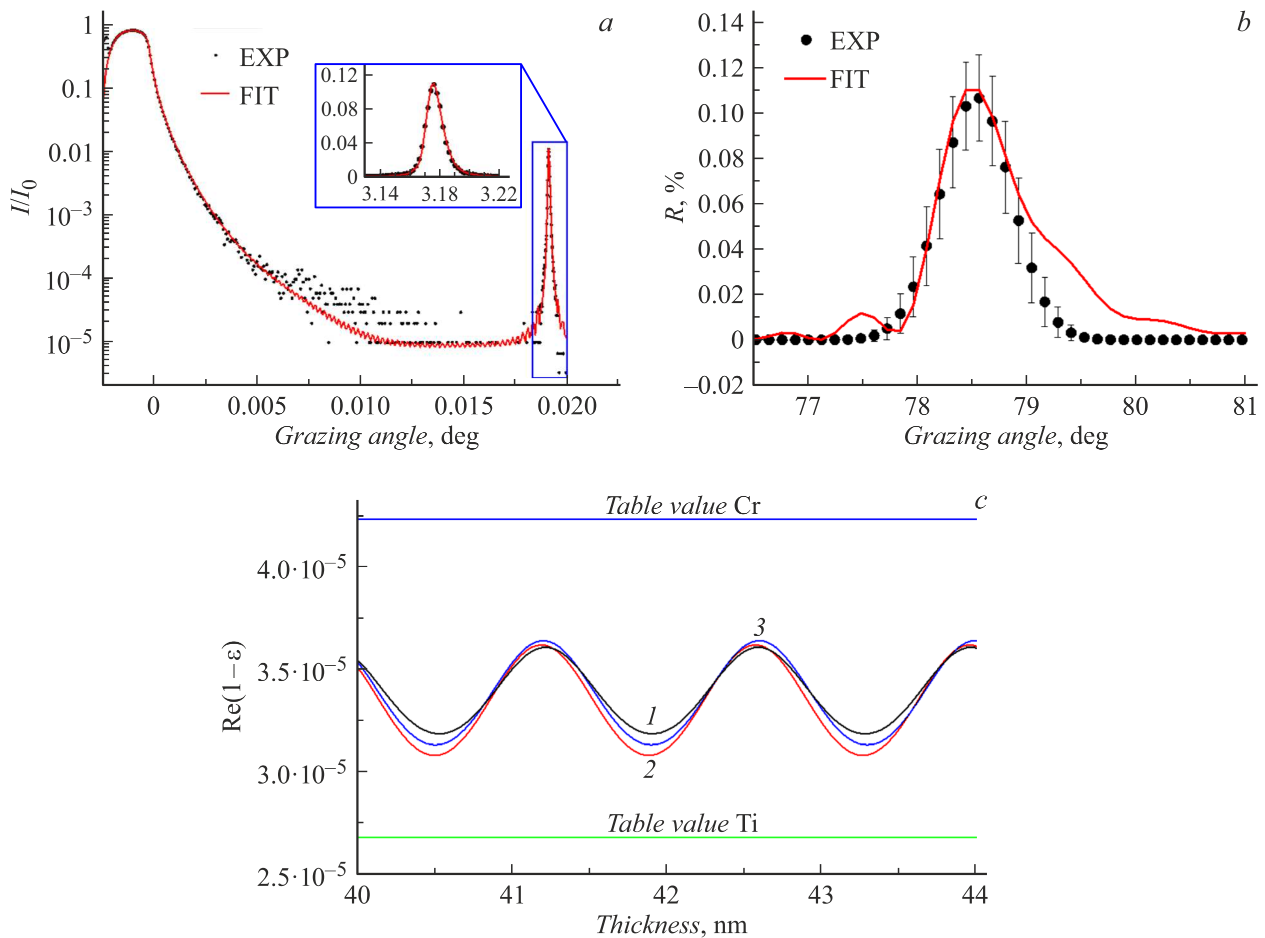

Figure 7. Experimental and theoretical dependences of the reflectivity of $Cr/B_4C/Ti$ MLS №5 at wavelengths of 0.154 (*a*) and 27.4 nm (*b*); dispersion allowance profiles to the real part of the dielectric permittivity: *1* — for Cr/Ti (MLS №1), *2* — $Cr/Ti/B_4C$ (MLS №2) and *3* — $Cr/B_4C/Ti$ (MLS №5) (*c*).

in a strong change of the layer densities relative to the table values: $\rho(\mathrm{Cr}) = 6.8\,\mathrm{g/cm^3}$, $\rho(\mathrm{Ti}) = 4.9\,\mathrm{g/cm^3}$ (see table).

The addition of B4C to any interface, as can be seen, results in an increase of the reflectivity of the MLS. However, the addition of buffer layers also leads to a decrease in the effective value of the reflecting layers N_{eff}, which is much greater in the case of deposition of B_4C on Ti. Fig. 6 shows the dependences of the reflection coefficient and the amount of N_{eff} on the thickness of B_4C buffer layers in the Cr/Ti MLS. The period drift in the growth process in this particular series of experiments can be a reason for such a change of N_{eff}.

The highest level of reflectivity $R \cong 11 \pm 2\%$ is achieved when the B_4C buffer layers with a thickness of 0.01 nm are deposited on denser Cr layers, and not less dense Ti layers, which is not typical for many MLS [19].

The reason for the increase of reflectivity, according to the reflection curves, is less mixing of the layers of the multilayer system with each other — the values of layer densities approach the tabular values (see table), which results in an increase of the jump of electron density at the interfaces. However, the width of the transition boundaries does not change. Figure 7 shows the dependences of the reflectivity at 0.154 (Fig. 7, *a*) and 27.4 nm (Fig. 7, *b*) on the MLS with the highest reflection coefficient of $R \cong 11 \pm 2\%$ — №5 ($Cr/B_4C/Ti$) and profiles of the dispersion allowance to the real part of the permittivity (Fig. 7, *c*) for MLS №1 (Cr/Ti), №2 ($Cr/Ti/B_4C$) and №5 ($Cr/B_4C/Ti$), showing how the introduction of B_4C interlayer results in sharper permittivity profiles in the multilayer structure. We explain this by the introduction of boron atoms into the Cr and Ti layers with the formation of borides in the transition region, which prevent the interaction of metals in the structure.

Conclusion

The paper covers the study of Cr/Ti MLS with B_4C buffer layers at different interfaces and without them. Cr/Ti MLS fabricated by magnetron sputtering initially had a reflection coefficient at the level of $R \cong 5\%$ at a wavelength of 2.74 nm. The reason for the lower reflection coefficient compared to the theoretical limit is the mixing of the materials of the multilayer system with each other, which

is why the layer densities are very different from the table values, which leads to a deterioration in optical contrast at the boundaries. Insertion thin buffer B_4C layers of the order of 1 Å to any interface results in an increase of reflectivity because of weaker mixing of the MLS layer materials among themselves, as a result of which the layer densities approach tabular values.

The greatest increase in the reflection coefficient to $R \cong 11 \pm 2\%$ is achieved by depositing B_4C buffer layers on denser Cr layers.

Funding

The study was supported financially by Russian Science Foundation grant №21-72-30029.

Conflict of interest

The authors declare that they have no conflict of interest.

References

[1] M. Schuster, H. Gobel. J. Phys. D: Appl. Phys., **28** (4A), A270 (1995). DOI: 10.1088/0022-3727/28/4A/053

[2] H. Mimura, S. Handa, T. Kimura, H. Yumoto, D. Yamakawa, H. Yokoyama, S. Matsuyama, K. Inagaki, K. Yamamura, Ya. Sano, K. Tamasaku, Y. Nishino, M. Yabashi, T. Ishikawa, K. Yamauchi. Nature Phys., **6** (2), 122 (2010). DOI: 10.1038/nphys1501

[3] J.B. Kortright, J.H. Underwood. Nucl. Instrum. Methods Phys. Res. Section A: Accelerators, Spectrometers, Detectors and Associated Equipment, **291** (1–2), 272 (1990). DOI: 10.1016/0168-9002(90)90073-F

[4] S.S. Andreev, M.S. Bibishkin, N.I. Chkhalo, A.Ya. Lopatin, V.I. Luchin, A.E. Pestov, K.A. Prokhorov, N.N. Salaschchenko. Nucl. Instrum. Methods Phys. Res. Section A: Accelerators, Spectrometers, Detectors and Associated Equipment, **543** (1), 340 (2005). DOI: 10.1016/j.nima.2005.01.252

[5] N.I. Chkhalo, M.N. Drozdov, E.B. Kluenkov, S.V. Kuzin, A.Ya. Lopatin, V.I. Luchin, N.N. Salashchenko, N.N. Tsybin, S.Yu. Zuev. Appl. Opt., **55** (17), 4683 (2016). DOI: 10.1364/AO.55.004683

[6] A.D. Akhsakhalyan, E.B. Kluenkov, A.Ya. Lopatin, V.I. Luchin, A.N. Nechay, A.E. Pestov, V.N. Polkovnikov, N.N. Salashchenko, M.V. Svechnikov, M.N. Toropov, N.N. Tsybin, N.I. Chkhalo, A.V. Shcherbakov. J. Surf. Investigation: X-ray, Synchrotron and Neutron Techniques, **11** (1), 1 (2017). DOI: 10.1134/S1027451017010049

[7] E. Fogelqvist, M. Kördel, V. Carannante, B. Önfelt. H.M. Hertz. Sci. Reports, **7** (1), 1 (2017). DOI: 10.1038/s41598-017-13538-2

[8] N. Ghafoor, P. Persson, J. Birch, F. Eriksson, F. Schäfers. Appl. Opt., **45** (1), 137 (2006). DOI: 10.1364/AO.45.000137

[9] Q. Huang, J. Fei, Y. Liu, P. Li, M. Wen, Ch. Xie, Ph. Jonnard, A. Giglia, Zh. Zhang, K. Wang, Zh. Wang. Opt. Lett., **41** (4), 701 (2016). DOI: 10.1364/OL.41.000701

[10] E.M. Gullikson, F. Salmassi, A.L. Aquila, F. Dollar. *Progress in Short Period Multilayer Coatings for Water WindowAapplications* (Lawrence Berkeley National Laboratory, 2008), http://escholarship.org/uc/item/8hv7q0hj

[11] M. Svechnikov. J. Appl. Crystallogr., **53** (1), 244 (2020). DOI: 10.1107/S160057671901584X

[12] N. I. Chhalo. *Metody diagnostiki strukturnyh i dispersionnyh svojstv mnogoslojnyh rentgenovskih zerkal* (Dissertatsiya, Nizhny Novgorod, 2009) (in Russian).

[13] Electronic source. Available at: https://xdb.lbl.gov/Section1/Table_1-3.pdf

[14] M. S. Bibishkin, I. G. Zabrodin, S. Yu. Zuev, E. B. Klyuenkov, N. N. Salashchenko, D. P. Chehonadsky, N. I. Chkhalo, L. A. Shmaenok. Poverkhnost. Rentgenovskie, sinkhrotronnye i nejtronnye issledovaniya, **1**, 70 (2003) (in Russian).

[15] M. S. Bibishkin, I. G. Zabrodin, E. B. Klyuenkov, N. N. Salashchenko, D. P. Chehonadskikh, N. I. Chkhalo. Poverkhnost. Rentgenovskie, sinkhrotronnye i neytronnye issledovaniya, **2**, 41 (2003) (in Russian).

[16] P.A. Grunow, L.E. Klebanoff, S. Graham Jr., S.J. Haney, W.M. Clift. Proceed. SPIE, **5037**, 418 (2003). www.oxfordxtg.com/products/micro.htm

[17] V.N. Polkovnikov, S.A. Garakhin, D.S. Kvashennikov, I.V. Malyshev, N.N. Salashchenko, M.V. Svechnikov, R.M. Smertin, N.I. Chkhalo. Tech. Phys., **65** (11), 1809 (2020). DOI: https://doi.org/10.1134/S1063784220110225

[18] V.N. Polkovnikov, R.A. Shaposhnikov, S.Yu. Zuev, M.V. Svechnikov, M.G. Sertsu, A. Sokolov, F. Schäfers, N.I. Chkhalo. Opt. Express, **30** (11), 19332 (2022). DOI: 10.1364/OE.448069

[19] R.A. Shaposhnikov, V.N. Polkovnikov, N.N. Salashchenko, N.I. Chkhalo, S.Yu. Zuev. Opt. Lett., **47** (17), 4351 (2022). DOI: 10.1364/OL.469260

[20] R.M. Smertin, N.I. Chkhalo, M.N. Drozdov, S.A. Garakhin, S.Yu. Zuev, V.N. Polkovnikov, N.N. Salashchenko, P.A. Yunin. Opt. Express, **30** (26), 46749 (2022). DOI: 10.3367/UFNr.2019.05.038623

Translated by A.Akhtyamov